SUPPORTING INFORMATION

Using confined self-adjusting carbon nanotube arrays as high-sensitivity displacement sensing element

Jae-Ik Lee, Youngkee Eun, Jungwook Choi, Dae-Sung Kwon, and Jongbaeg Kim *

School of Mechanical Engineering, Yonsei University
134 Shinchon-Dong, Seodaemun-Ku, Seoul 120-749, Republic of Korea

Email: kimjb@yonsei.ac.kr

★Author to whom correspondence should be addressed. Email: kimjb@yonsei.ac.kr

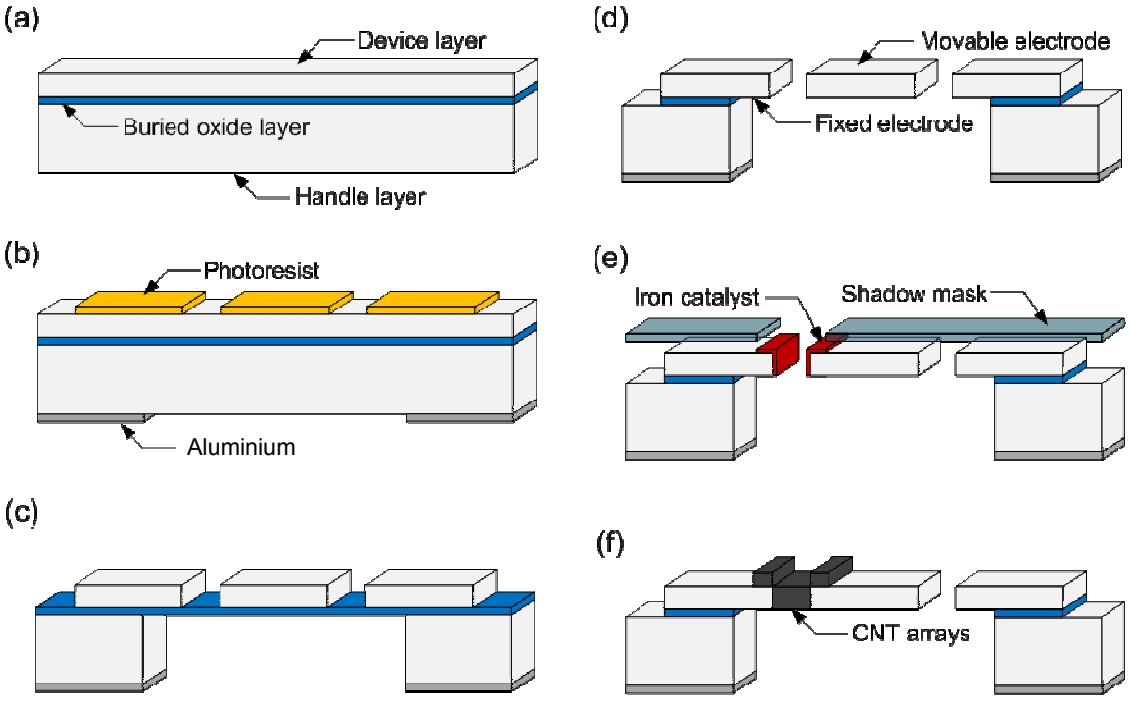

Figure S1. Detailed fabrication process of VACNT-based displacement sensor.

(a) The silicon microstructures of the VACNT-based displacement sensor were fabricated on a silicon-on-insulator wafer using a 20-μm-thick device layer, 520-μm-thick handle layer, and 1-μm-thick buried oxide layer. The device layer was heavily doped with arsenic of resistivity 0.005 Ω cm.

(b) The etch masking of the front and back sides was lithographically defined.

(c) The device and handle layers were etched by deep reactive ion etching.

(d) The buried silicon oxide layer was wet-etched using hydrofluoric acid.

(e) A 5-nm-thick layer of iron catalyst was deposited by electron beam evaporation. The patterning of the catalyst layer was done using a separately prepared shadow mask.

(f) The CNT arrays were synthesized by thermal chemical vapour deposition process.

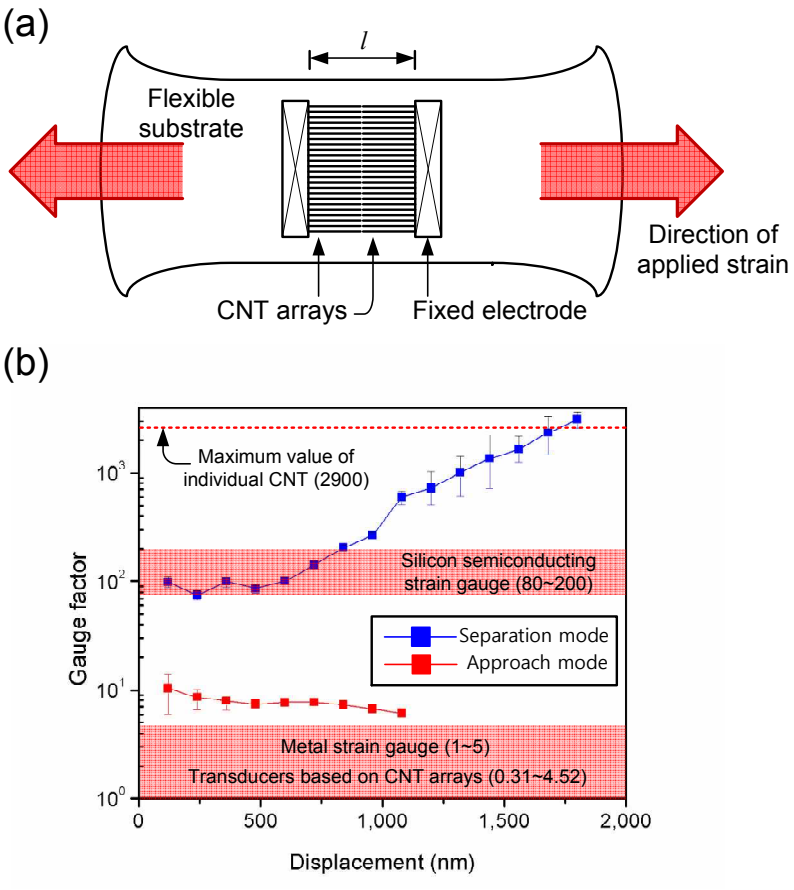

Figure S2. Comparison of sensitivities of the proposed VACNT-based displacement sensor and a piezoresistive sensor.

The figure of merit of a piezoresistive sensor is expressed in terms of the gauge factor (GF), which is given by GF = $\Delta R/R\varepsilon$, where ΔR is the change in the resistance R for an applied strain ε. To compare the sensitivity of the proposed VACNT-based displacement sensor with that of a piezoresistive sensor, we calculated the corresponding GF of the former. Assuming that the displacement sensor is indirectly used to measure the strain of a flexible substrate (Fig. S2a), the applied strain is obtained from $\Delta l/l$, where Δl is the change in the gap l. Using the experimentally determined change in the contact resistance in the separation mode (Fig. 3a), we calculated the corresponding GFs as a function of the displacement (Fig. S2b), and determined the maximum GF to be 3115, which corresponded to a displacement of 2.1 μm. In the approach mode, a maximum GF of 10 was obtainable. Although the GF in the approach mode was substantially lower than that in the separation mode, it was still higher than those of other CNT-array-based mechanical sensors, which range from 0.31 to 4.52. [1-4]

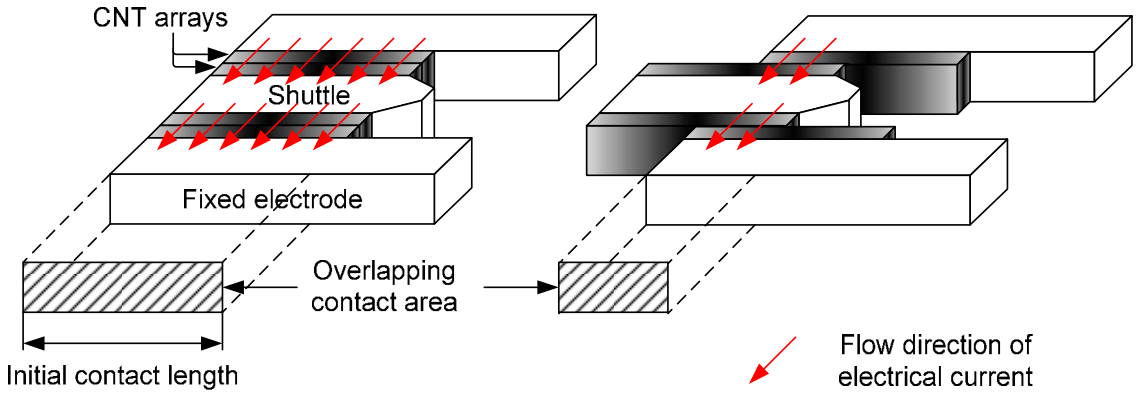

Figure S3. Linear output current signal in the sliding mode.

When the shuttle moves leftwards, the overlapping contact area of the VACNTs for electrical current flows decreases and the electrical resistance of the two fixed electrodes increases.[5] Because the change in the overlapping contact area is directly proportional to the displacement of the shuttle and the electrical conductivity of the contacting CNTs, the output electrical signal can be estimated.

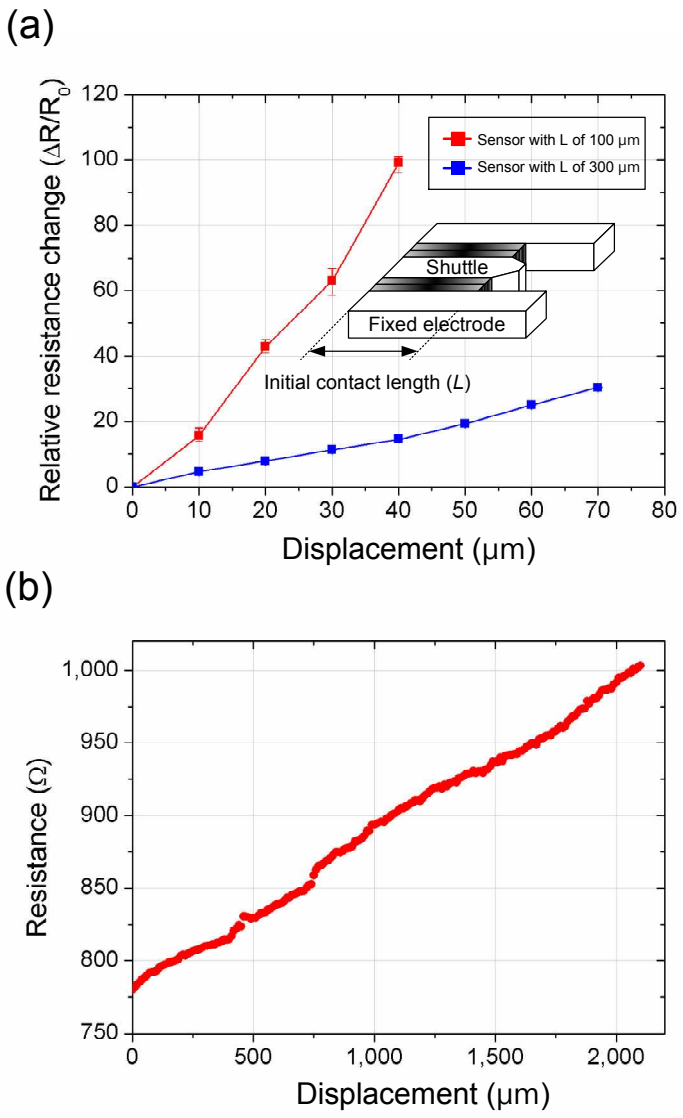

Figure S4. The sensitivity and maximum sensing range in the sliding mode

The sensitivity and maximum sensing range can be adjusted by varying the initial contact length of the CNTs (*L*). Figure S5a shows the measurement results of two sensors having different values of the initial CNT contact length (*L*). A greater variation of the percentage change in the resistance for identical displacements was observed for a CNT length of 100 μm than for a length of 300 μm. It is noteworthy that the initial overlapping CNT contact length determines the maximum sensing range, which enables the measurement of a much wider range of displacements. In this study, displacement sensing was conducted up to 2.1 mm, as shown in Fig. S5b.

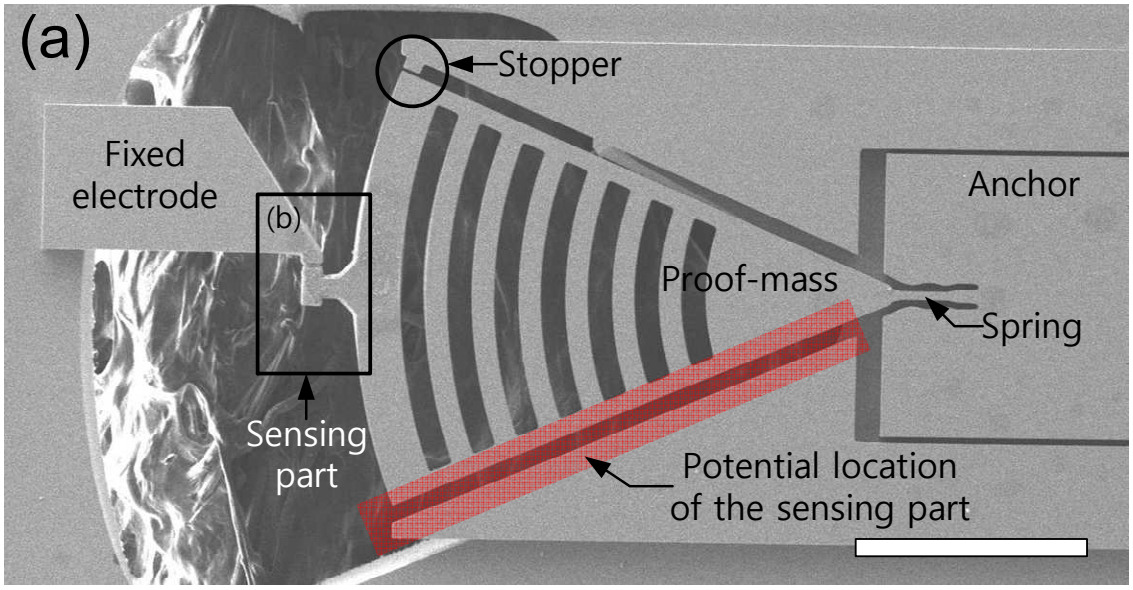

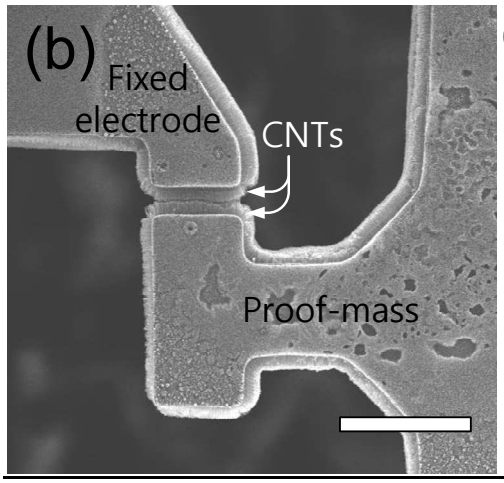

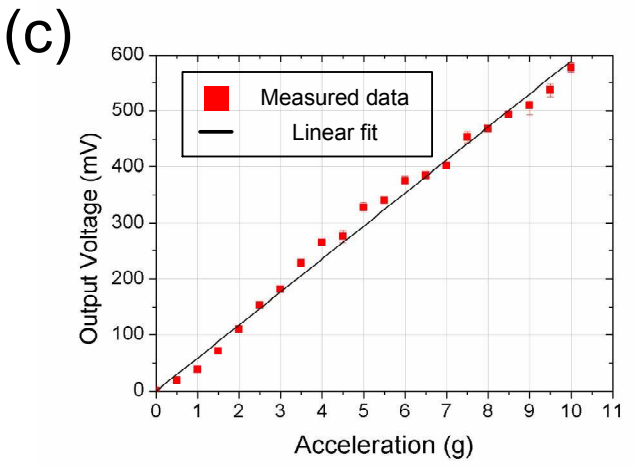

Accelerometer	Sensitivity (mV/g/V)	1st Resonant frequency (kHz)	Figure of merit
Sankar, A. R. *et al* [7]	0.135	2.89	1.13
Huang, S. *et al* [8]	21.2	1.115	26.36
Partridge, A. *at al* [9]	3	0.7	1.47
The presensted accelerometer	**11.68**	**2.07**	**50.05**

Figure S5. Design and demonstration of 1-axis accelerometer

As an example of a mechanical sensor, we developed a 1-axis accelerometer. As shown in Fig. S5a (scale bar: 500 μm), a proof mass was anchored to a compliant spring, and a stopper was used to prevent excessive displacement of the proof mass, which would permanently deform the CNTs.[6] The sensing part was positioned at the end of the proof mass (Fig. S5b; scale bar: 50 μm). The measured changes in the contact resistance of the CNT arrays with

respect to the accelerations are shown in Fig. S5c as the voltage outputs obtained by a Wheatstone bridge circuit. From the linear fit, the sensitivity was calculated to be 11.68 mV/g/V. As shown in the table, by using the proposed high-sensitivity displacement sensor, the accelerometer could achieve higher sensitivity and resonant frequency than other accelerometers using a resistive bridge circuit. The figure of merit is given by Sf_0^2, where S denotes the minimum sensitivity and f_0 denotes the first resonant frequency.[10,11]

The area artificially coloured red in Fig. S5a is also a potential location of the sensing part, and the sensitivity and maximum sensing acceleration can be tuned by controlling the distance between the sensing part and the anchor. The closer the sensing part to the anchor, the higher is the maximum sensing acceleration. This is because the contacting CNTs are completely separated at high accelerations. Conversely, when the sensing part is far from the centre of rotation, maximum changes in displacement can be achieved, and hence high sensitivity. This design flexibility that allows for tuning the sensitivity and maximum sensing acceleration without degradation of the resonant frequency is an advantage of the proposed device over piezoresistive transducers, in which the sensing elements can only be placed at the highly strained locations.

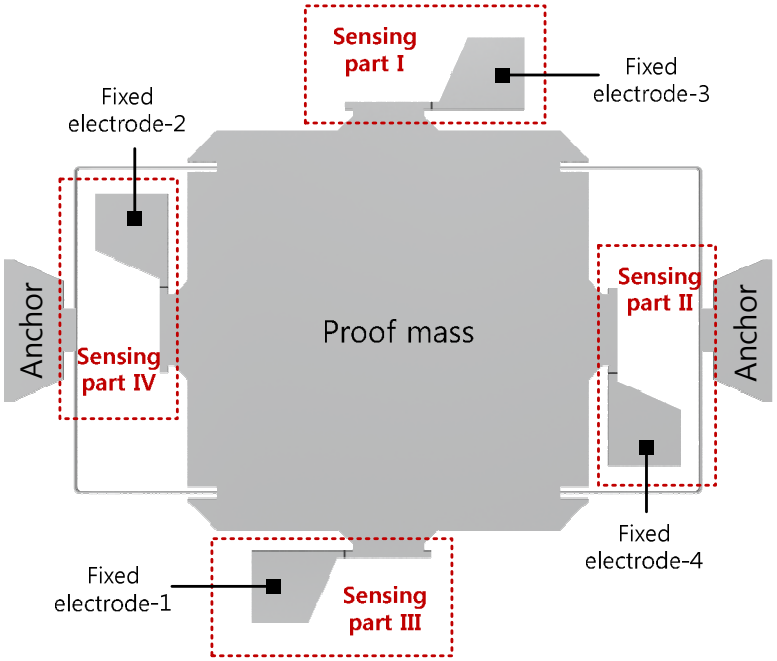

	SP I		SP II		SP III		SP IV	
+ Ax	Separation	+	Sliding	+	Approach	-	Sliding	+
– Ax	Approach	-	Sliding	+	Separation	+	Sliding	+
+ Ay	Sliding	+	Approach	-	Sliding	+	Separation	+
– Ay	Sliding	+	Separation	+	Sliding	+	Approach	-
Az	Sliding	+	Sliding	+	Sliding	+	Sliding	+

Figure S6. Sensing modes and changes in contact resistance for accelerations in different directions. (SP: sensing part; +: increase in resistance; -: decrease in resistance).

	Sensitivity (mV/g/V)			1st Resonant frequency (kHz)	Figure of merit
	A_x	A_y	A_z		
Amarasinghe, R. *et al* [12]	0.228	0.23	0.196	1.432	0.40
Plaza, J. A. *et al* [13]	0.16	0.093	0.464	0.715	0.24
Hsieh, H. -S. *at al* [14]	0.17	0.17	0.12	1.57	0.30
Dong, P. *at al* [15]	0.00217	0.00225	0.00264	164	0.36
The presensted accelerometer	**0.301**	**0.296**	**0.300**	**2.572**	**1.98**

Figure S7. Comparison of performance of proposed 3-axis accelerometer with those of piezoresistive accelerometers of previous studies.

REFERENCES

(S1) Bsoul, A.; Ali, M. S. M.; Nojeh, A.; Takahata, K. Piezoresistive Strain Sensing using Carbon Nanotube Forests Suspended by Parylene-C Membranes. *Appl. Phys. Lett.* **2012**, *100*, 213510.

(S2) Yilmazoglu, O.; Popp, A.; Pavlidis, D.; Schneider, J. J.; Garth, D.; Schuttler, F.; Battenberg, G. Vertically Aligned Multiwalled Carbon Nanotubes for Pressure, Tactile and Vibration Sensing. *Nanotechnology* **2012**, *23*, 085501.

(S3) Lee, B. Y.; Heo, K.; Bak, J. H.; Cho, S. U.; Moon, S.; Park, Y. D.; Hong, S. Scalable Assembly Method of Vertically-suspended and Stretched Carbon Nanotube Network Devices for Nanoscale Electro-mechanical Sensing Components. *Nano Lett.* **2008**, *8*, 4483–4487.

(S4) Pushparaj, V. L.; Ci, L.; Sreekala, S.; Kumar, A.; Kesapragada, S.; Gall, D.; Nalamasu, O.; Ajayan, P. M.; Suhr, J. Effects of Compressive Strains on Electrical Conductivities of a Macroscale Carbon Nanotube Block. *Appl. Phys. Lett.* **2007**, *91*, 153116.

(S5) Lee, J. I.; Choi, J.; Lee, K.; Jeong, B.; Kim, J. Development of Carbon Nanotubes Contact-based Linear Displacement Sensor with Large Sensing Range. *Proc. IEEE 23rd Int. Conf. on Micro Electro Mechanical Syst. (MEMS)*, **2010**, 627–630.

(S6) Lee, J. I.; Eun, Y.; Jung, H. I.; Choi, J.; Kim, J. A Novel Accelerometer Based on Contact Resistance of Integrated Carbon Nanotubes. *Proc. IEEE 24th Int. Conf. on Micro Electro Mechanical Syst. (MEMS)*, **2011**, 533–536.

(S7) Sankar, A. R.; Lahiri, S. K.; Das, S. Performance Enhancement of a Silicon MEMS Piezoresistive Single Axis Accelerometer with Electroplated Gold on a Proof Mass. *J.*

Micromech. Microeng. **2009**, *19*, 025008.

(S8) Huang, S.; Li, X.; Song, Z.; Wang, Y.; Yang, H.; Che, L.; Jiao, J.; A High-performance Micromachined Piezoresistive Accelerometer with Axially Stressed Tiny Beams *J. Micromech. Microeng.* **2005**, *15*, 993-1000.

(S9) Partridge, A.; Reynolds, J. K.; Chui, B. W.; Chow, E. M.; Fitzgerald, A. M.; Zhang, L.; Maluf, N. I.; Kenny. T. W. A High-performance Planar Piezoresistive Accelerometer *J. Microelectromech. Syst.* **2000**, *9*, 58-66.

(S10) Yazdi, N.; Ayazi, F; Najafi, K. Micromachined Inertial Sensors. *Proc. IEEE* **1998**, *86*, 1640-1659.

(S11) Crescini, D.; Marioli, D.; Taroni, A. Low-cost Accelerometers: Two Examples in Thick-Film Technology. *Sens. Actuators, A* **1996**, *55*, 79-85.

(S12) Amarasinghe, R.; Dao, D. V.; Toriyama, T.; Sugiyama, S. Simulation, Fabrication and Characterization of a Three-axis Piezoresistive Accelerometer. *Smart Mater. Struct.* **2006**, *15*, 1691-1699.

(S13) Plaza, J. A.; Chen, H.; Esteve, J.; Lora-Tamayo, E. New Bulk Accelerometer for Triaxial Detection. *Sens. Actuators, A* **1998**, *66*, 105-108.

(S14) Hsieh, H.; Chang, H.; Hu, C.; Cheng, C.; Fang, W. A Novel Stress Isolation Guard Ring Design for the Improvement of a Three-axis Piezoresistive Accelerometer. *J. Micromech. Microeng.* **2011**, *21*, 105006.

(S15) Dong, P. Li, X.; Yang, H.; Bao, H.; Zhou, W.; Li, S.; Feng, S. High-performance Monolithic Triaxial Piezoresistive Shock Accelerometers. *Sens. Actuators, A* **2008**, *141*, 339-346.